Analysis of the Information Capacity of Neuronal Molecular Communications Under Demyelination and Remyelination

Geoflly L. Adonias, Conor Duffy, Michael Taynnan Barros, *Member, IEEE*, Claire E. McCoy, and Sasitharan Balasubramaniam, *Senior Member, IEEE*

***Abstract*— Demyelination of neurons can compromise the communication performance between the cells as the absence of myelin attenuates the action potential propagated through the axonal pathway. In this work, we propose a hybrid experimental and simulation model for analyzing the demyelination effects on neuron communication. The experiment involves locally induced demyelination using *Lysolecithin* and from this, a myelination index is empirically estimated from analysis of cell images. This index is then coupled with a modified Hodgkin-Huxley computational model to simulate the resulting impact that the de/myelination processes has on the signal propagation along the axon. The effects of signal degradation and transfer of neuronal information are simulated and quantified at multiple levels, and this includes (1) compartment per compartment of a single neuron, (2) bipartite synapse and the effects on the excitatory post-synaptic potential, and (3) a small network of neurons to understand how the impact of de/myelination has on the whole network. By using the myelination index in the simulation model, we can determine the level of attenuation of the action potential concerning the myelin quantity, as well as the analysis of internal signalling functions of the neurons and their impact on the overall spike firing rate. We believe that this hybrid experimental and *in silico* simulation model can result in a new analysis tool that can predict the gravity of the degeneration through the estimation of the spiking activity and vice-versa, which can minimize the need for specialised laboratory equipment needed for single-cell communication analysis.**

***Index Terms*— Re/Demyelination, Lysolecithin (LPC), Hodgkin-Huxley model, myelination index, molecular communications.**

Manuscript received September 2, 2021; revised November 30, 2021; accepted December 9, 2021. Date of publication December 21, 2021; date of current version January 13, 2022. This work was supported in part by the Science Foundation Ireland (SFI) for the CONNECT Research Centre under Grant 13/RC/2077, in part by the SFI Future Research Leader Award under Grant 16/FRL/3855, and in part by the Irish Research Council (IRC) Postgraduate Scholarship under Grant GOIPG/2018/2648. The work of Michael Taynnan Barros was supported by the European Union's Horizon 2020 Research and Innovation Programme through the Marie Skłodowska-Curie under Grant 839553. *(Corresponding author: Geoflly L. Adonias.)*

Geoflly L. Adonias is with the Walton Institute for Information and Communication Systems Science, Waterford Institute of Technology, Waterford, X91 KOEK Ireland (e-mail: geoflly.adonias@waltoninstitute.ie).

Conor Duffy is with the School of Pharmacy and Biomolecular Science, Royal College of Surgeons in Ireland, Dublin 2, D02 YN77 Ireland (e-mail: conorduffymct@rcsi.ie).

Michael Taynnan Barros is with the School of Computer Science and Electronic Engineering, University of Essex, Colchester CO4 3SQ, U.K., and also with CBIG/BioMediTech, Tampere University, 33014 Tampere, Finland (e-mail: m.barros@essex.ac.uk).

Claire E. McCoy is with the School of Pharmacy and Biomolecular Science, and FutureNeuro, Royal College of Surgeons in Ireland, Dublin 2, D02 YN77 Ireland (e-mail: clairemccoy@rcsi.ie).

Sasitharan Balasubramaniam is with the School of Computing, University of Nebraska–Lincoln, Lincoln, NE 68588 USA (e-mail: sasi@unl.edu).

Digital Object Identifier 10.1109/TNSRE.2021.3137350

I. Introduction

WITH the ever-growing knowledge of the biological processes involved in the regeneration of nerve tissues, a better understanding of these events is crucial for the creation of more robust models that could accelerate the development of targeted therapeutics against neurodegeneration [1]. For example, multiple sclerosis (MS) is an autoimmune demyelinating disease (DD), characterised by localised destruction of protective myelin sheaths around axons and subsequent impairment of neuronal function and action potential (AP) propagation, leading to the formation of sclerotic plaques across the central nervous system (CNS). In relapse-remitting MS (RRMS), demyelination is caused by abnormal peripheral immune invasion of the CNS and inflammatory attack against the myelin sheath, most notably from activated T-cells [2]. This form of the disease is characterised by "attacks" (relapse), followed by periods of recovery (remitting), where innate repair mechanisms of the CNS restore damaged myelin in a process known as **remyelination**. However, MS can also manifest in the form of primary progressive MS (PPMS), where demyelination is continuous and remyelination mechanisms appear to be dysfunctional [3]. It is, therefore, of considerable interest to develop therapies that can promote or restore remyelination, with current research approaches including stem cell therapeutics, biomaterial construct implants and nanoparticle or extracellular vesicle treatment formulations, among others [4]–[7].

The drug *Lysolecithin* (LPC) has been widely used for years to experimentally induce demyelination in neurons from both the central and peripheral nervous systems (PNS). Many studies have taken advantage of LPC to help characterise experimental models in terms of its morphology by light and electron microscopy, electrophysiology and biochemistry. The various uses and validity of organotypic cerebellar slice cultures in studying demyelinating disease have been thoroughly reviewed by Doussau and colleagues [9], identifying the culture system as the easiest way to replicate the various stages of myelination, demyelination and remyelination that are of interest outside of *in vivo* models. These cultures

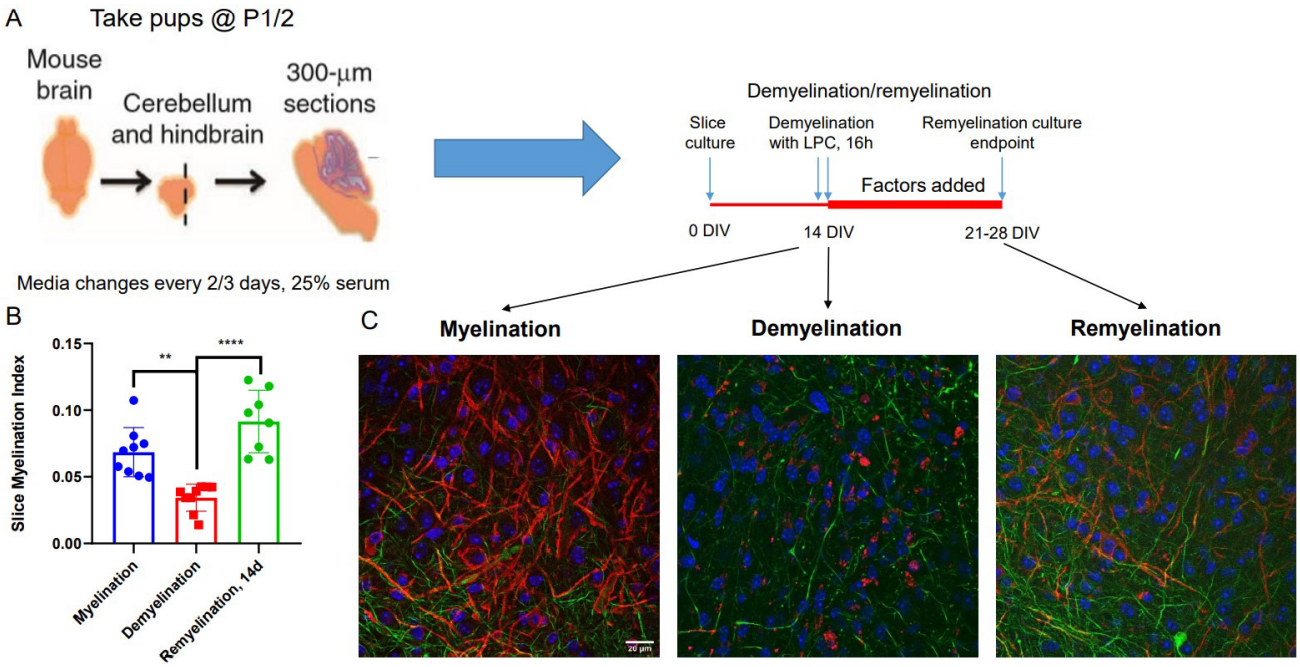

Fig. 1. (A) Schematic of organotypic brainstem and cerebellum slice culture model set-up. Drawings of mouse brains borrowed from Miron *et al.* [8]. (B) Average myelination indices of slices in myelination, demyelination and remyelination conditions. Each datapoint represents the index of a single slice. ** = $p < 0.01$, **** = $p < 0.0001$, one-way ANOVA with post-hoc Sidak's multiple comparisons test. Graph generated in GraphPad Prism. (C) Representative images of myelination, demyelination and remyelination staining under confocal microscopy, composite images. Blue = DAPI, Green = NFH, Red = MBP.

faithfully retain the cytoarchitecture and neuronal networks of the cerebellar cortex *in vitro* for weeks to months, allowing for long-term investigations of novel therapeutics and sufficient recovery time following a demyelinating insult to observe remyelination. Furthermore, the neurons in these slice cultures retain electrophysiological characteristics, such as Purkinje cells forming new synapses with targets upon stimulation [10]. Crucially to study remyelination, cells at all stages of the oligodendroglia lineage are retained in the organotypic cerebellar slice culture [11].

Turning to LPC specifically, this was first demonstrated to induce demyelination in organotypic cerebellar slice cultures by Birgbauer and colleagues in 2004, as observed by immunostaining for myelin basic protein (MBP), myelin oligodendrocyte glycoprotein (MOG), and 2′, 3′-cyclic nucleotide 3′-phosphodiesterase (CNPase), followed by recovery and subsequent remyelination [12]. This approach to inducing demyelination has been used in several studies to date, including a demonstration that the MS therapy fingolimod can promote remyelination [13], validation of an immune-mediated technique for inducing demyelination [14] and characterization of the critical pro-remyelination properties of microglia [8], [15]. Furthermore, focal injections of LPC to the spinal cord (Fig. 1) are a frequently-used *in vivo* model of demyelination [16], thus using an LPC-based *in vitro* model is attractive to screen potential treatments before commencing *in vivo* studies.

The findings on the demyelination and remyelination processes observed with the help of the wet-lab experiments will allow the construction of a more refined and accurate computational simulation model and, possibly, shine light on the way neurons encode information. In the last few years, there has been an increasing number of scientists that started to look at alternative coding techniques, some of them imposing profound implications on the field of neural computation [17]. **Firing rate coding** [17], [18] is a technique where the rate with which spikes are being fired is proportional to the strength of the stimuli. Several other coding techniques have also been proposed as alternatives such as rank order coding or sparse coding, where these techniques take into account that real neurons use spikes that are followed by refractory periods which should play a role in information encoding. One of the simplest techniques proposed is to just count the number of action potentials fired during a particular period, and this is referred to as **count coding** [17]. With this coding technique, the maximum amount of information transmitted by N neurons is $\log_2(N+1)$ bits. Another alternative method is to check for the presence of an action potential in a specific time window. In this technique, the presence of a firing will be considered a bit "1" and its absence a bit "0," and this is referred to as **binary coding** [17], [19]. For a binary code, the maximum amount of information transmitted by N neurons is equal to $\log_2(2^N)$ bits. More complex encoding techniques have also been proposed. Such approaches use the precise time of each spike on each input to increase the maximum amount of information transmitted by a group of neurons. In this case, the maximum amount of information transmitted by N neurons in a time window of t ms, where the spikes can be timed with a precision of 1 ms, is $N \cdot \log_2(t)$ bits. Thus, this encoding technique is known as **temporal coding** or **timing coding** [17], [20].

This model should be able to play a significant role in the analysis of the impact that demyelination and remyelination will have on the neuronal signalling communication process

and should also be used to add a new analysis tool for wet-lab experimentalists without the need for specialised equipment. This hybrid computational simulation and experimental model has the potential to improve both sides of the study and bring together scientists and researchers from different disciplines by unifying their findings and validating their data for a more reliable analysis of the demyelination and remyelination processes on the molecular aspect of neuronal communications.

The objective of this paper is to computationally validate the data collected from wet-lab experiments on LPC-induced demyelination and to analyse its impact on the communication once the demyelinated neuron is partially remyelinated. The contributions of this paper are:

- **A novel hybrid wet-lab-computational model:** We describe the construction of a wet-lab dataset of myelination under conditions of LPC-induced demyelination and subsequent remyelination, alongside undisturbed myelination controls, suitable for input to a computational model. By utilising a method of analysis from neuronal molecular communications, we use this hybrid model to understand the signal propagation behaviour as they propagate through the axonal pathway.
- **Modelling of the spiking rate for myelin-deficient neurons:** As proposed in the literature, spike firing usually follows a *Poisson* process [21], [22]. The rate and pattern of firing can defer between different demyelination intensities leading to the modelling of their respective behaviour into known distributions.
- **Multi-perspective theoretical analysis of LPC-induced demyelination:** Communication metrics (e.g., channel capacity, attenuation and time delay) analysis are presented and discussed on the effects of demyelination from three different perspectives, (1) single neuron and the signal propagation through axonal compartments, (2) bipartite synapse and the effects on the excitatory post-synaptic potential and, (3) small neuronal network of 27 cells is analysed to determine the network communication when a neuron starts to demyelinate.

The remainder of this paper is as follows in Section II we present the methodologies applied for both the wet-lab experiments and the computational simulations for analysis and validation of data from LPC-induced demyelination. In Section III, we present and discuss our results from (1) single neuron, (2) bipartite synapse and (3) small neuronal network perspectives and, finally, in Section IV, we conclude this analysis and discuss potential future works.

II. Materials and Methods

A. LPC-Induced Demyelination

1) Animals and Tissue Preparation: All experiments were conducted in accordance with EU and Health Products Regulatory Authority guidelines. A breeding colony of wild-type C57BL/6J mice was maintained in the Biomedical Research Facility in the Royal College of Surgeons in Ireland using mice obtained from The Jackson Laboratory. Organotypic brain slice cultures of the brainstem and cerebellum were established to examine demyelination and remyelination *ex vivo*, based on the protocol described by Doussau and colleagues [9]. Briefly, the cerebellum and brainstem were cut into slices 300 μm thick along the sagittal axis using a McIlwain Tissue Chopper. Slices were separated in slice culture media (46.55% Minimum Essential Medium (MEM), 25% heat-inactivated horse serum, 25% Earl's balanced salt solution, 1% glutamine, 1% 100 U/mL P/S, 1.45% glucose 45, final concentration 6.5 mg/mL) and transferred onto 0.4 μm Millipore mesh membrane inserts inside 6-well plates containing 1 mL of slice culture media. Typically 6-7 slices were obtained per brain, and the slices from each brain were distributed across separate wells, with 6 slices per culture well. Slices were then cultured at 37 °C, 5% oxygen, with fresh slice culture media, exchanged every 2-3 days, for a total of 14 days *in vitro* (d.i.v.).

2) Demyelination and Remyelination: To induce demyelination, the drug lysolecithin (LPC) was applied to 14 d.i.v. cultures at a concentration of 0.5 mg/mL for 16 hours. LPC was then withdrawn, the cultures were washed once in slice culture media before being transferred and maintained in fresh media for a 24-hour recovery period. Slices were then allowed to remyelinate for a further 14 days *in vitro*, with media changes every 2-3 days as before.

3) Immunofluorescence and Fluorescent Microscopy: Immunofluorescent staining and fluorescent microscopy were used to evaluate the extent of myelination in organotypic brain slice cultures. Cultures were washed once in PBS before fixation with 4% paraformaldehyde solution (PFA) for 45 minutes, at which point PFA was withdrawn and cultures ready for staining. Cultures were first blocked for 3 hours using a 2% horse serum, 10% goat serum, 1% BSA, 0.25% Triton-X-100, 1 mM HEPES solution in PBS at room temperature. The mesh insert membranes were then cut and slices transferred to 24-well plates for staining. Primary antibodies for anti-NFH (1:2000) and anti-MBP (1:600) were then applied in the block solution, 400 μL/well for 2 days at 4 °C. Slices were then washed with shaking three times at room temperature in PBS-0.01% Triton-X-100, 1 hour per wash, before applying AlexaFluor secondary antibodies - 1:500 anti-chicken AlexaFluor 488, 1:500 anti-rat AlexaFluor 568, in block solution, 400 μL/well overnight at 4°C. Slices were then counterstained with DAPI –1:30,000 of stock in PBS, 500 μL per well – for ten minutes before washing three times in PBS-0.01% Triton-X-100 as before. Slices were mounted with ProLong Gold and were labelled with randomly generated 6-digit numbers corresponding to treatment or control conditions, to introduce blinding during image acquisition.

Slices were imaged using a Zeiss 710 confocal microscope at 40x magnification. Three representative image stacks were acquired per slice, using Z-stack imaging at 0.5 μm intervals across 10 μm. Images were then analysed in ImageJ for co-localisation of MBP to NFH (neurofilament protein H) to assess the extent of myelination in each slice. A myelination index (ι_{my}), ranging from 0 to 1, was calculated for each z-stack by dividing the amount of co-localisation by the total amount of NFH, and averages for each slice calculated by pooling myelination indices from representative images together. The indices obtained are, therefore, a measure of myelin sheaths overlaid on axon fibres, relative to total axon

density. A graphical illustration of tissue analysis and slice culture model set-up are shown in Fig. 1, with a description of the culture set-up, the timeline for introducing LPC for demyelination at day 14, and the stop point for remyelination in Fig. 1(a). Taking the average myelination index for each slice we confirm that introduction of LPC for 16h produced a significant decrease in myelination, allowing a 14-day recovery period following LPC withdrawal, we observed a significant restoration of myelin sheaths in the remyelination conditions as measured by the myelination index relative to demyelination slices, Fig. 1(b). Representative images for each condition are also shown for illustrative purposes in Fig. 1(c). As can be seen in the "Myelination" image, prior to application of LPC clear (red) myelin sheaths can be observed overlaid on (green) axons. Following LPC application, substantially less myelin stain can be observed in the "Demyelination" image, and what myelin is present does not form clear sheath structures, most likely debris. In the "remyelination" image, taken 14 days following LPC withdrawal, myelin in sheath structures can be observed again laid over axons, though perhaps less pronounced or thinner than the myelination condition. This is an expected characteristic of repaired myelin sheaths. It is therefore clear that the myelination index measurement is reflective of clear differences in myelination of axons. For that reason, for computational analysis, indices were restricted to the top 3.5 μm of each 10 μm stack captured across slices and conditions which, visually, it is clear that NFH staining was of superior quality in the regions of the slice closer to the surface, as seen in Fig. 2.

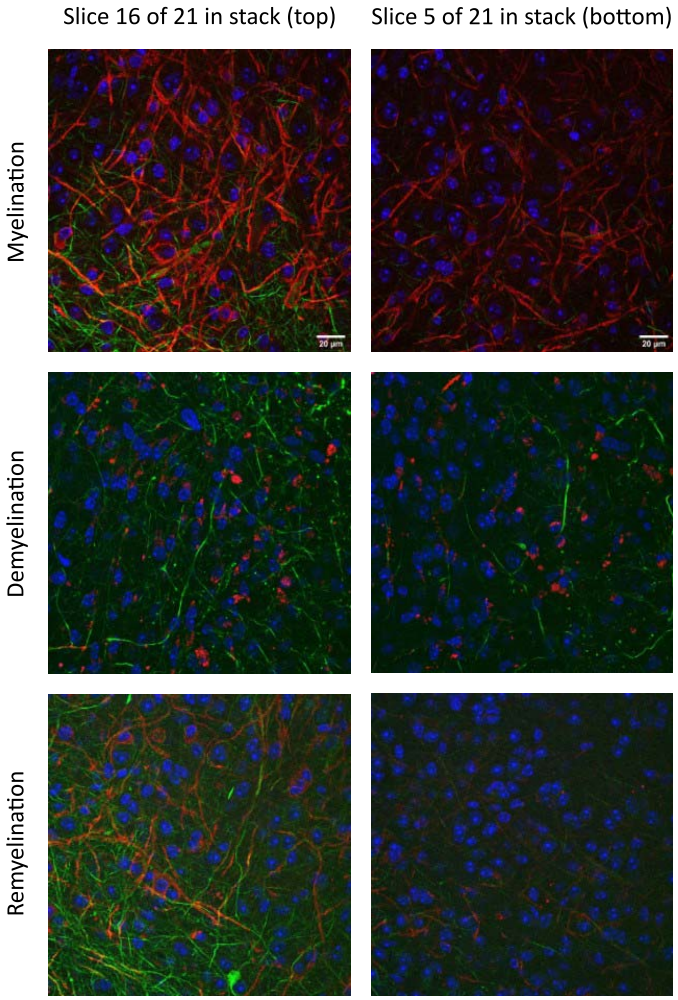

Fig. 2. Comparison of staining quality at the top (slice 16 of 21, 2.5 μm below surface) and bottom (slice 5 of 21, 8 μm below surface) of image stacks under confocal microscopy. Composite images, Blue = DAPI, Green = NFH, Red = MBP.

B. Computational Model for Axonal Demyelination

The axon under analysis in this work is modelled according to the Hodgkin-Huxley formalism [23] with modifications proposed by Quandt and Davis [24], as depicted in Fig. 3, where the parameters are described in Table I.

When an external stimulus, I_{ext}, is applied, it triggers either the activation or inactivation of the ionic channels that allow the exchange of ions that result in depolarisation (or hyperpolarize when it is inhibited) of the membrane of the cell. These dynamic changes in the voltage and current of each ion diffusion through the membrane are modelled as

$$C\frac{\mathrm{d}V}{\mathrm{d}t} = -I_l - I_{Na} - I_K - I_{syn} + I_{ext}, \tag{1}$$

where V is the membrane potential, I_x are the ionic currents, where x represents either a specific ion (Na, K) or the leak channel (l). Those currents are represented as

$$I_l = g_l(V - E_l), \tag{2}$$
$$I_{Na} = g_{Na}m^3h(V - E_{Na}), \tag{3}$$
$$I_K = g_K n^4(V - E_K), \tag{4}$$

where m and h are the activation and inactivation variables of the sodium (Na) channel, respectively, and n is the activation variable of the potassium (K) channel. Following the approach proposed by Hodgkin and Huxley [23], those variables are represented below as x and their dynamics are described as

$$\frac{\mathrm{d}x}{\mathrm{d}t} = \alpha_x(V)\ (1 - x) - \beta_x(V)\ x, \tag{5}$$

in which the values of the rate constants α_i and β_i for the i-th ionic channel can be defined as

$$\alpha_m = \frac{0.1(V + 40)}{1 + e^{-(V+40)/10}}, \tag{6}$$
$$\beta_m = 4e^{-(V+65)/20}, \tag{7}$$
$$\alpha_h = 0.07e^{-(V+65)/20}, \tag{8}$$
$$\beta_h = \frac{1}{1 + e^{-(V+35)/10}}, \tag{9}$$
$$\alpha_n = \frac{0.01(V + 55)}{1 - e^{-(V+55)/10}}, \tag{10}$$
$$\beta_n = 0.125\ e^{-(V+65)/80}. \tag{11}$$

We also integrated a process into the model for the synaptic inputs from pre-synaptic cells in which the ionic channels that are activated will release neurotransmitters that are diffused into the synaptic cleft towards neuroreceptors at the post-synaptic cell. This relationship is represented as

$$I_{syn} = g_{syn}(V - E_{syn}), \tag{12}$$

where the synaptic conductance, g_{syn}, and the synaptic reversal potential, E_{syn}, are used to describe many different types of

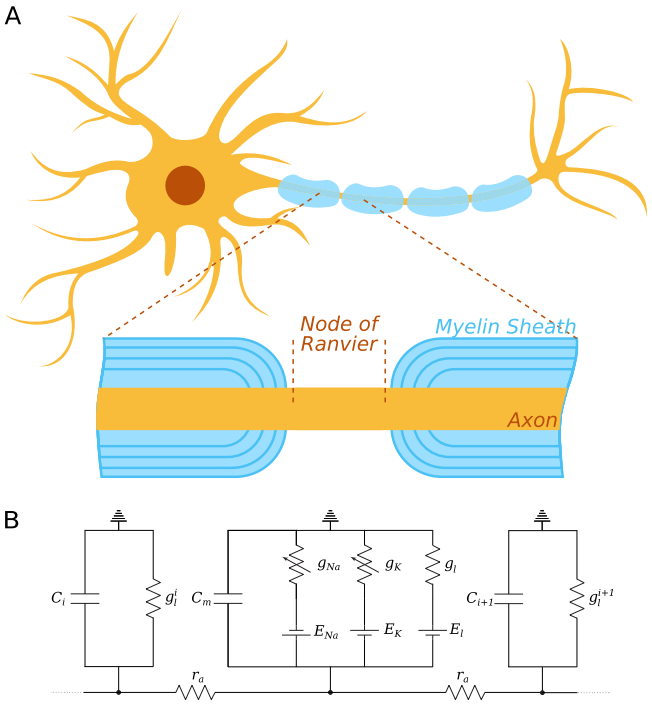

Fig. 3. Illustration of an axonal pathway with a (A) detail of a *Node of Ranvier* and two internodes, respectively, (B) Hodgkin-Huxley circuit model with parameter detailed description provided in Section II-B; the parameters C_i and g_l^i and their subsequent myelinated compartments are described by equations (14) and (15), respectively.

TABLE I
SUMMARY OF ELEMENTS AND PARAMETERS FOR MODELLING AND SIMULATION

Element	Value	Unit
Membrane capacitance (C_m)	1	μF/cm^2
Axon radius (δ_a)	5	μm
Node length (L_n)	4	μm
Internodal distance (d_i)	2	mm
Internal resistance (r_a)	100	Ω·cm
Myelin sheath (w)	200	wraps
Sodium reversal potential (E_{Na})	53	mV
Potassium reversal potential (E_K)	-74	mV
Leak reversal potential (E_l)	-60	mV
Sodium conductance density (G_{Na})	1200	mS/cm^2
Potassium conductance density (G_K)	90	mS/cm^2
Leak conductance density (G_l)	20	mS/cm^2
Internodal membrane conductance (g_i)	0.3	mS/cm^2
Temperature (T)	37	°C
Time step (dt)	0.25	μs
Q_{10}	3.0	-

synapses, and the latter may assume different values according to the types of neuroreceptors. The four major transmitters used for communication in the nervous systems are listed in Table II [25], [26].

The g_{syn} can be described as a superposition of exponentials and is represented as

$$g_{\text{syn}} = \sum_f \bar{g}_{\text{syn}}\, \mathrm{e}^{-(t-t^{(f)})/\tau}\, H(t-t^{(f)}), \tag{13}$$

where τ is a time constant, $\bar{g}_{\text{syn}}$ is the peak synaptic conductance, $t^{(f)}$ is the arrival time of a pre-synaptic action potential and $H(\cdot)$ is the Heaviside step function [25]. As we have

TABLE II
E_{syn} FOR DIFFERENT RECEPTORS

Neurotransmitter	Neuroreceptor	E_{syn} (mV)
Glutamate	Non-NMDA	0
Glutamate	NMDA	0
GABA	GABA_A	−70
GABA	GABA_B	−100

investigated in [27], the membrane potential that reaches the pre-synaptic terminals can affect the probability of releasing neurotransmitters. Consequently, anything that would affect this potential could also indirectly lead to changes in the release of neurotransmitters. In other words, it is not only the synaptic current (Equation (12), but also all other ionic currents that can influence the release of neurotransmitters and consequently compromise the integrity of the signal being propagated down the neuronal network.

The modifications, proposed by Quandt and Davis [24], on the original Hodgkin-Huxley model is to incorporate the dynamics of myelination and understand the signal propagation per compartment, by including the capacitance of the internode (C_i), which is represented as

$$C_i = \frac{2\,\pi\,\delta_a\, d_i\, C_m}{\iota_{my}\, w + 1}, \tag{14}$$

and the assumption that the internode have a specific leak conductance (g_l^i), which is represented as

$$g_l^i = \frac{2\,\pi\,\delta_a\, d_i\, g_i}{\iota_{my}\, w + 1}, \tag{15}$$

where ι_{my} is the myelination index described in Section II-A3. The myelinated compartments (also called internode compartments) are modelled as not having ionic channels. This is mainly because as the myelin sheath provides insulation, it also blocks the ionic channels in the axonal membrane, not allowing the free movement and exchange of ions between intra- and extra-cellular mediums. Furthermore, both the C_i and g_l^i values are heavily influenced by the number of myelin wraps, w, as shown in equations (14) and (15) and, as w decreases due to demyelination, it negatively impacts the speed and potential responses concerning the propagation of the signal.

An axon with six internodes and seven nodes of *Ranvier* was built as illustrated in Fig. 3. The simulations were conducted using the NEURON simulation environment with Python [28], [29]. Each point of stimulation was set at 200 spikes per second following a *Poisson* process [22] unless otherwise stated. Five simulations were conducted for each value of ι_{my} starting at full myelination (100%) and decreasing at 12.5% intervals until it reaches 12.5%, hereafter considered as full demyelination (see Section II-A). Each spike is represented as a bit '1' and its absence is represented as a bit '0' in a specific time slot. In this work, the time slot for sampling the neuronal binary information is 5 ms. This is short enough to detect less than a single spike and account for its refractory periods. The cells were connected following a standard procedure with the `NetCon` object that defines a synaptic

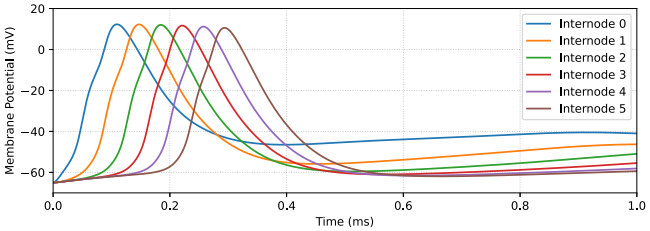

(a) Action potential propagation on an axon fully myelinated.

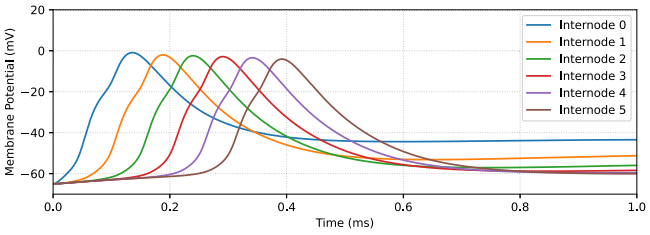

(b) Action potential propagation on an axon with half of its normal myelination levels.

Fig. 4. Parallel for action potential propagations between a fully myelinated and a partially (50%) demyelinated axon.

connection. We are not using any morphological-type-related connection probability as the neurons are modelled in a generic structure and behaviour. The network arrangement does not follow any structure in particular, e.g. cortical layers, instead it was arranged in a cubic shape (more details in Section III-D) where there was a single synapse per connection and, a single connection where needed.

III. Results and Discussion

A. Demyelination and Remyelination of Slice Cultures

Following the 16-hour treatment with 0.5 mg/mL LPC, we observed a significant reduction in the myelination of neurons as determined by the average myelination index of slices relative to untreated controls ($p < 0.01$, one-way ANOVA and Sidak's multiple comparisons posthoc test). LPC-induced demyelination was observed to be of a similar magnitude in our hands as reported by several other groups [13], [14], [30]. Following 14 days of recovery post-LPC-induced demyelination in brain slice media, remyelination was observed that was significantly greater than the demyelination time-point as determined by the myelination index ($p < 0.0001$, one-way ANOVA and Sidak's multiple comparisons posthoc test).

The average myelination index of each slice was used to determine the success and overall extend of LPC-induced demyelination and remyelination; however, individual myelination indices of each captured image were also recorded as part of the analysis process.

B. Compartmental Analysis

To understand the dynamics of action potential propagation in the axonal pathway, our modelling process should account for the effects of myelinated and non-myelinated sections of the axon. For that reason, we are using the multi-compartmental modelling framework [31] to help put together a detailed representation of the axon that would provide us with enough information regarding the electrical behaviour of the neuronal membrane.

In this work, we have modelled the axon with Hodgkin-Huxley compartments for the nodes of *Ranvier* and the myelinated internode compartments. As indicated in Section II-B, even though both use the same framework, the internodes are modelled slightly differently to account for the myelin sheaths. Then, we decided to start our analysis on the neuron itself, in other words, on the behaviour of the membrane per compartment (Fig. 4). The model used follows the description from Section II-B aiming to understand how partially myelinated neurons, i.e. under either demyelination or remyelination conditions, affects the propagation of action potentials per neuronal compartment. Fig. 4 shows how a neuron with half of its normal myelin, Fig. 4(b), compared to a fully myelinated neuron shown in Fig. 4(a). The results depicts not only a delay for the action potential to reach its peak in all compartments but also shows how damages to the myelin sheath can affect the value of membrane potential reached. For that reason, we decided to numerically evaluate by how much the shift in peak time and amplitude changes as the demyelination worsens and, analogously, the changes due to remyelination processes.

1) Relative Mean Shift: Visually, we first noticed subtle shifts in amplitude (peak potential reached by the membrane) and in time (spikes were taking longer to reach their peak values). We then decided to quantify these shifts, both in amplitude and in time, on average, by proposing a metric that we called **relative mean shift**. For the analysis on time shift, we consider the points in time where each spike peaked at the input as T_{in}^k, where $k = \{1, 2, 3, \ldots, K\}$ identifies the order of each spike and, T_{out}^k as the peak times at the output. Thus, we define the relative mean time shift, $\overline{\delta_t}$ (ms), as

$$\overline{\delta_t} = \frac{1}{K}\sum_{k=1}^{K}(T_{out}^k - T_{in}^k). \tag{16}$$

Analogously, we can define the relative mean amplitude shift, $\overline{\delta_v}$ (mV), with V_{in}^k and V_{out}^k as the peak amplitudes of spike k at the input and output, respectively.

As illustrated in Fig. 5, the difference in the average membrane potential in relation to a full myelinated neuron is considerably damaging to the signal propagation through the axonal pathway. At 12.5% myelination, the difference is almost 60 mV shown in Fig. 5(a) and this is enough to not even consider the signal travelling down the axon as a spike. The degradation in the membrane potential is not linear, where its logarithmic-shaped curve illustrates a much steeper degeneration for the lower half of the indices when compared to the upper half as the mean shift in amplitude starts to plateau as it approaches full myelination. Analogous to the effects on membrane potential, Fig. 5(b) shows how the peak times of the action potentials are delayed as ι_{my} decreases. The negative-exponentially-shaped curve depicts a smoother increase in the mean time shift for higher indices. Both results in Fig. 5 match findings in Cohen *et al.* [32], where they identified longer onset latencies and lower peak amplitudes in the conduction

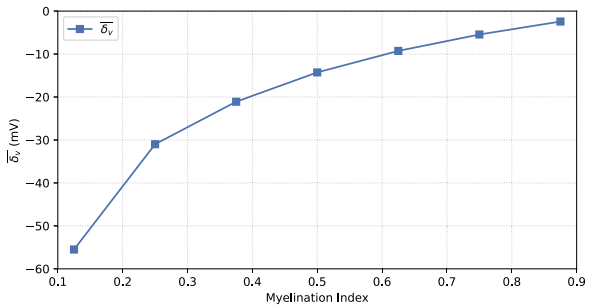

(a) Relative mean amplitude (potential) shift.

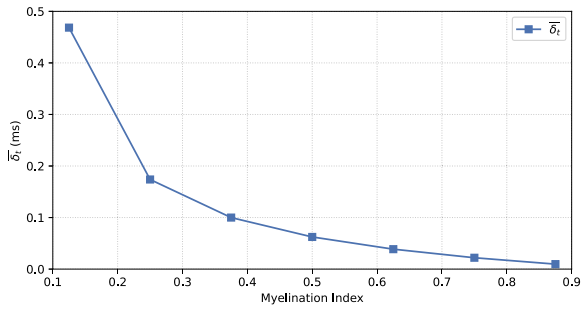

(b) Relative mean time shift.

Fig. 5. Relative mean shift in relation to a fully myelinated neuron.

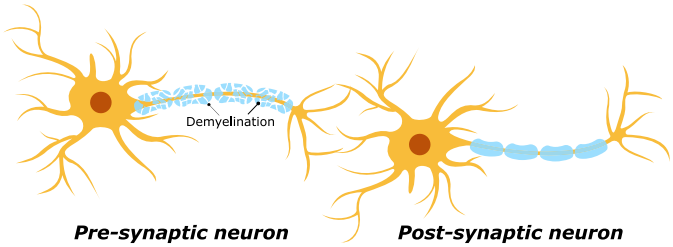

Fig. 6. Bipartite synapse with demyelinated pre-synaptic neuron.

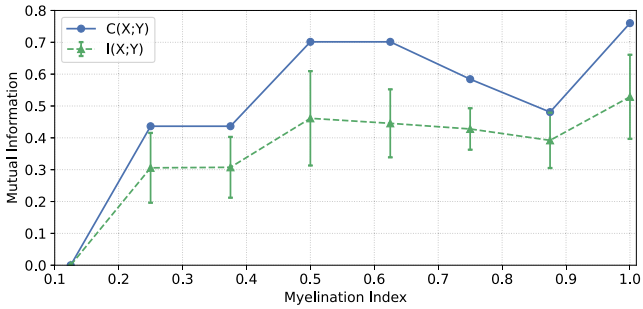

Fig. 7. Capacity, C(X; Y) and mean mutual information, I(X; Y), for peer-to-peer analysis of a pre-synaptic demyelinated neuron.

of action potentials along myelinated axons on models of L5 pyramidal cells.

C. Bipartite Synapse Analysis

From the perspective of information and communication theory, the neuron can be seen as peers in the nervous system characterising a peer-to-peer communication system [33]. Even though the bit transmission may be affected by the refractory period of a recently fired action potential, depending on the intensity of the stimuli, new bits may still be transmitted during relative refractory periods. Furthermore, if the post-synaptic neuron does not manage to evoke a subsequent action potential, there will be no waiting queue [26] which characterises the channel as *memoryless*. This means that any spike not propagated, because the post-synaptic neuron is unable to fire at the time the pre-synaptic stimuli arrives, will be lost. A pair of neurons, one acting as the transmitter, known as pre-synaptic neuron and, the other acting as the receiver, called a post-synaptic neuron, form a bipartite synapse as shown in Fig. 6. A synaptic connection between only two neurons is considered a single input single output (SISO) communication channel [22] and can be evaluated as such using well-known metrics from information and communication theory such as capacity [34], [35].

1) Channel Capacity: Shannon's entropy of a discrete random variable x and probability mass function $p(x)$ can be used in biological systems to represent information as bits in several processes and is defined as

$$H(X) = -\sum_{x \in X}^{P}(x)\log_2 p(x), \tag{17}$$

where $X = \{x_0, x_1\}$.

Additionally, the definition of conditional entropy is based on the conditional and joint distribution of x and y:

$$H(X|Y) = -\sum_{x \in X}\sum_{y \in Y} p(x, y)\log_2 p(x|y), \tag{18}$$

where $Y = \{y_0, y_1\}$.

All the remaining probabilities are defined as follows:

$$p(x) = p(x = x_0) + p(x = x_1), \tag{19}$$

$$p(y) = [p(y = y_0) + p(y = y_1)]\, p(y|x), \tag{20}$$

$$p(y = y_0|x = x_0) = 1 - p(y = y_1|x = x_0), \tag{21}$$

$$p(y = y_0|x = x_1) = 1 - p(y = y_1|x = x_1). \tag{22}$$

In other words, we could characterise the destructive effects of demyelination on the propagation of the signal as the probability of receiving a bit '0,' i.e. no spike, given that a bit '1' was sent at the input, $p(y = y_0|x = x_1)$ in Eq. (22). Moreover, as the remyelination takes place, there is an increase on the probability of receiving a bit '1,' given that a bit '1,' i.e. spike, was sent, $p(y = y_1|x = x_1)$ in Eq. (22). This shows how the channel capacity can be affected as the conditional probabilities for receiving a specific bit changes with the degeneration and, eventually the partial regeneration of the myelin sheath.

The mutual information between two variables indicates that the input can be construed as a measure of the "noise" in the channel given the output, and is calculated as

$$I(X; Y) = H(X) - H(X|Y)$$
$$= -\sum_{x \in X}\sum_{y \in Y} p(x)p(y|x)\log_2 \frac{p(y|x)}{p(y)}, \tag{23}$$

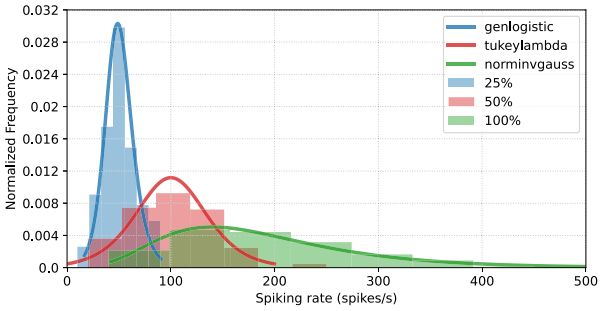

(a) Spiking rate distributions for different ι_{my}.

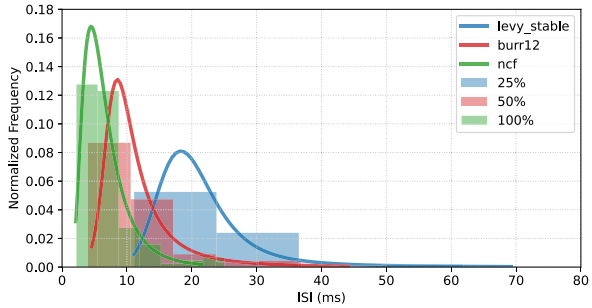

(b) Interspike intervals (ISI) distributions for different ι_{my}.

Fig. 8. Distributions for spiking rate and interspike intervals revealing a shift in peak and widening of the curve for different myelination indices.

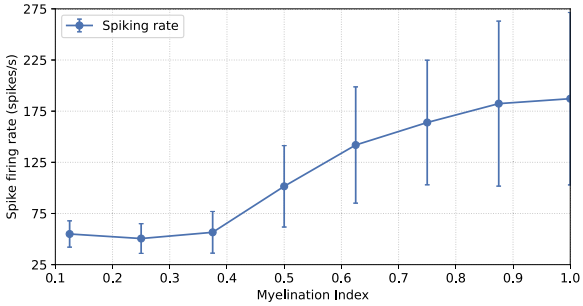

(a) Mean and standard deviation for spiking rate on a small neuronal network.

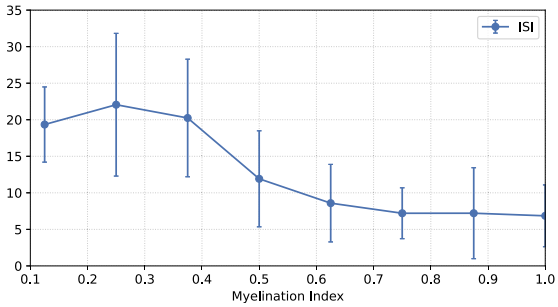

(b) Mean and standard deviation for interspike intervals on a small neuronal network.

Fig. 9. Mean and standard deviation for spiking rate and interspike intervals for the analysis of a network of 27 neurons.

and the maximum average mutual information in any single use of the channel, known as capacity, which is represented as

$$C(X;Y) = max_{p(x)} I(X;Y). \tag{24}$$

From our simulations, both the capacity and mean mutual information are shown in Fig. 7.

As shown in Fig. 7, there are a few fluctuations which we believe to be due to the randomness of the spikes at the input of a myelinated axon. The mutual information increases in a way that resembles a logarithmic curve, similar to the mean shift in amplitude from Fig. 5(a) and corroborates findings from Veletić *et al.* [33], [36]. The authors showed a similar growth of channel capacity (bits), and information rate (bits per second) which is proportional to capacity values for bipartite synaptic connections.

D. Network Analysis

When part of a larger network, neurons can receive stimuli from several other neurons and pass this information down to many other neurons as well characterising a multiple-input and multiple-output (MIMO) communication channel [37]. For our network analysis, we arranged 27 neurons in a $3 \times 3 \times 3$ cubic structure, with vertical and horizontal connections, but not diagonals; this was a design choice to avoid too much noise at higher spike firing frequencies and still takes advantage of a good connectivity scheme. As with any stochastic system, it is not ideal to force a system's behaviour into a deterministic model, where we need to account for inherent randomness. In this scenario, the system is our network and as the demyelination gets worse, the spike-firing pattern and rate is negatively compromised. In this scenario, all 27 neurons are demyelinated at the same time and the same proportion, to mimic the process of demyelination for the calculation of ι_{my}, where all neurons in the field of view are demyelinated together.

1) Distribution Fitting: Several works in the literature have hypothesised that neurons follow a *Poisson* process when firing individually, but this may not be the case depending on the connectivity, stimulus and neuronal structure [38]. To assess these conditions, we turn to distribution fitting to help us understand how those differences affect the network as a whole and to reproduce its behaviour. This modelling technique is most commonly done by applying the Kolmogorov–Smirnov (KS) test for goodness of fit [39]. Once the best fit is found for the data, both the histogram of the real data and the probability distribution function, f_x, of the best-fitted distribution are plotted together as shown in Fig 8.

Full myelination in Fig. 8(a) shows similarities to the findings by Platkiewicz and Brette [40] on the threshold for spike initiation which suggests that our results for different levels of demyelination can be a good representation for the validity of *in vivo* and *in vitro* experiments. Furthermore, we have also found strong similarity between our results in Fig. 8(b) and the results presented by Levine and Shefner [41]. Visually, the highly skewed distribution of their data resembles our findings for a *Noncentral F distribution* (n.c.f.) at full myelination. As for the spiking rate, these results suggest our models offer good approximations to provide complementary analysis tool

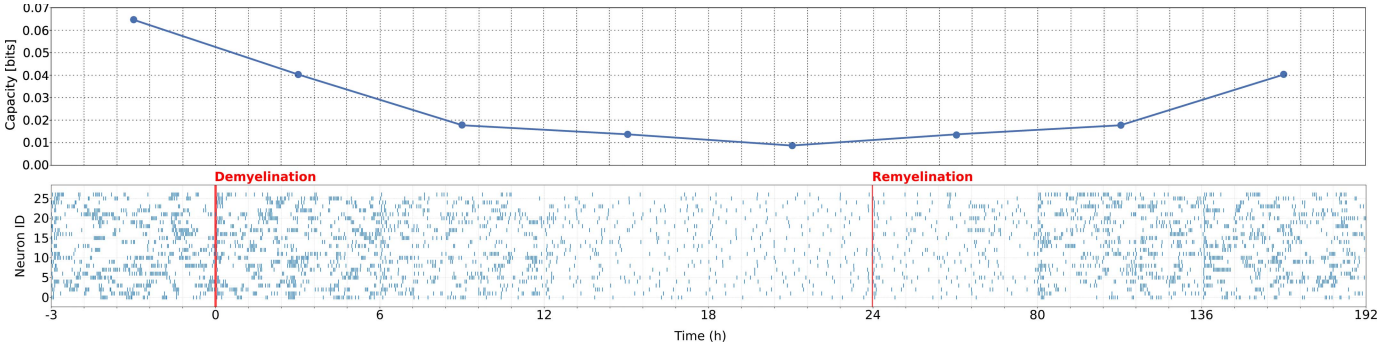

Fig. 10. Raster plots for different myelination indices showing how capacity is degrated and then regenerated as demyelination and remyelination take place over time.

of understanding internal signal propagation properties of the neurons under de/remyelination.

2) Spiking Rate and Interspike Intervals (ISI): One of the first things to indicate changes have happened in the neuronal communication channel is the spiking rate and the ISI. The spiking rate changes with the intensity of the stimulus as a way of encoding and modulating the stimulus with different firing frequencies. However, as neurons inside a network start to attenuate the signal or not pass it along altogether, it affects the rate with which the information is transferred within the network.

To understand what happens to the overall spiking rate inside a network, we decided to calculate its mean and standard deviation as the myelination index changed. As aforementioned in Section II, the myelination index was calculated for several neurons within the field of view for each cortical slice. For that reason, we chose to vary the index and see its effect on the entire network as depicted in Fig. 9.

As expected, Fig. 9(a) shows an increase in the spike firing rate as the myelination index increases. From myelination index of 0.375 onwards it is clear how it increases as a logarithmic-shaped curve, similar to the relative mean amplitude shift, $\overline{\delta}_v$, from Fig. 5(a). However, there is barely any difference for the three lowest index points. This is an interesting finding from the point of view of communication performance, where myelination index ι_{my} lower than 40% results in information that may be degraded to their worst levels and this change does not differ all the way to the level of 15%. In Fig. 10, it is possible to follow the visual decrease in spiking activity as demyelination progresses up to a point when the remyelination takes over and the restoration of several axonal pathways returns to propagate the action potentials. As the spiking rate is visually affected, so is the channel capacity which follows a similar behaviour as the one depicted in Section III-C, Fig. 7.

Researchers have already shown that action potentials are broadened and the conduction velocity supported by the saltatory nature of the conduction of neuronal potential is prone to failure as the myelin sheath gets more and more damaged [27], [32], [42]. All of the results available in the literature help support our claim that the frequency-dependent spiking activity is highly correlated to the level of demyelination which eventually plateau in both ends, as shown in Fig. 9, where values of ι_{my} less than 0.4 (lower index band) and greater than 0.7 (upper index band) show very subtle variations in comparison to values between 0.4 and 0.7 (middle index band).

IV. Conclusion

In this work, we have proposed a new hybrid computational simulation and experimental model to analyze signal propagation along neurons as they undergo demyelination and remyelination. We have analysed the effects of demyelination for three different levels and this includes (1) a single compartment within an axon, (2) bipartite synapse to understand how signal propagation changes as they propagate to the post-synaptic neuron and, (3) the impact of de/remyelination on a neuronal network. Our computational simulations were based on data from wet-lab experiments that used LPC to induce demyelination in slices of the cortical regions of the brain. The results from our computational simulations validated other findings from the literature that suggested the neuronal communication is indeed affected by demyelination. This analysis is based on developing a computational simulation model proposed by Hodgkin-Huxley and integrating it with signalling behaviour that is affected by the changes in the myelin sheaths. Our correlated analysis to the results from literature includes the changes in the amplitude and mean-shift, as well as capacity of information bits propagated between neurons, and the firing spike rate within a network of neurons as they undergo demyelination and remyelination. These approaches could pave the way for novel analytical techniques of neurons that are affected by diseases and their impact on their communication behaviour, by linking the results from wet-lab experiments that can feed into computational simulation models. This in turn can minimize the need for specialized experimental equipment that is needed to investigate changes in the communication behaviour, where the simulation model can provide very fine-grain signalling properties down to the compartment level, as well as between neurons, all the way up to the scale of the network.

Acknowledgment

The authors would like to thank Prof. Anna Williams' laboratory for developing and kindly sharing the ImageJ macro for the analysis of co-localisation of MBP to NFH.

REFERENCES

[1] W.-J. Huang, W.-W. Chen, and X. Zhang, "Multiple sclerosis: Pathology, diagnosis and treatments," *Experim. Therapeutic Med.*, vol. 13, no. 6, pp. 3163–3166, Jun. 2017.

[2] C. S. Constantinescu and B. Gran, "The essential role of T cells in multiple sclerosis: A reappraisal," *Biomed. J.*, vol. 37, no. 2, pp. 34–40, Mar./Apr. 2014.

[3] S. Faissner, J. R. Plemel, R. Gold, and V. W. Yong, "Progressive multiple sclerosis: From pathophysiology to therapeutic strategies," *Nature Rev. Drug Discovery*, vol. 18, no. 12, pp. 905–922, Dec. 2019.

[4] H.-B. Fan *et al.*, "Transplanted miR-219-overexpressing oligodendrocyte precursor cells promoted remyelination and improved functional recovery in a chronic demyelinated model," *Sci. Rep.*, vol. 7, no. 1, p. 41407, Feb. 2017.

[5] C. P. Duffy and C. E. McCoy, "The role of MicroRNAs in repair processes in multiple sclerosis," *Cells*, vol. 9, no. 7, p. 1711, Jul. 2020.

[6] U. Milbreta *et al.*, "Scaffold-mediated sustained, non-viral delivery of miR-219/miR-338 promotes CNS remyelination," *Mol. Therapy*, vol. 27, no. 2, pp. 411–423, Feb. 2019.

[7] A. P. Robinson *et al.*, "Nanocatalytic activity of clean-surfaced, faceted nanocrystalline gold enhances remyelination in animal models of multiple sclerosis," *Sci. Rep.*, vol. 10, no. 1, p. 1936, Feb. 2020.

[8] V. E. Miron *et al.*, "M2 microglia and macrophages drive oligodendrocyte differentiation during CNS remyelination," *Nature Neurosci.*, vol. 16, no. 9, pp. 1211–1218, Sep. 2013.

[9] F. Doussau, J.-L. Dupont, D. Neel, A. Schneider, B. Poulain, and J. L. Bossu, "Organotypic cultures of cerebellar slices as a model to investigate demyelinating disorders," *Expert Opinion Drug Discovery*, vol. 12, no. 10, pp. 1011–1022, Oct. 2017.

[10] T. Miki, H. Hirai, and T. Takahashi, "Activity-dependent neurotrophin signaling underlies developmental switch of Ca^{2+} channel subtypes mediating neurotransmitter release," *J. Neurosci.*, vol. 33, no. 48, pp. 18755–18763, Nov. 2013.

[11] A. M. Ghoumari, E. E. Baulieu, and M. Schumacher, "Progesterone increases oligodendroglial cell proliferation in rat cerebellar slice cultures," *Neuroscience*, vol. 135, no. 1, pp. 47–58, Jan. 2005.

[12] E. Birgbauer, T. S. Rao, and M. Webb, "Lysolecithin induces demyelination *in vitro* in a cerebellar slice culture system," *J. Neurosci. Res.*, vol. 78, no. 2, pp. 157–166, Oct. 2004.

[13] V. E. Miron *et al.*, "Fingolimod (FTY720) enhances remyelination following demyelination of organotypic cerebellar slices," *Amer. J. Pathol.*, vol. 176, no. 6, pp. 2682–2694, Jun. 2010.

[14] A. J. Pritchard, A. K. Mir, and K. K. Dev, "Fingolimod attenuates splenocyte-induced demyelination in cerebellar slice cultures," *PLoS ONE*, vol. 9, no. 6, Jun. 2014, Art. no. e99444.

[15] A. F. Lloyd *et al.*, "Central nervous system regeneration is driven by microglia necroptosis and repopulation," *Nature Neurosci.*, vol. 22, no. 7, pp. 1046–1052, Jul. 2019.

[16] N. D. Jeffery and W. F. Blakemore, "Remyelination of mouse spinal cord axons demyelinated by local injection of lysolecithin," *J. Neurocytol.*, vol. 24, no. 10, pp. 775–781, Oct. 1995.

[17] S. J. Thorpe, A. Delorme, and R. VanRullen, "Spike-based strategies for rapid processing," *Neural Netw.*, vol. 14, nos. 6–7, pp. 715–725, 2001.

[18] J. Gautrais and S. Thorpe, "Rate coding versus temporal order coding: A theoretical approach," *BioSystems*, vol. 48, nos. 1–3, pp. 57–65, 1998.

[19] M. R. DeWeese and A. M. Zador, "Binary coding in auditory cortex," in *Proc. 17th Conf. Neural Inf. Process. Syst.*, 2003, pp. 117–124.

[20] K. Aghababaiyan, V. Shah-Mansouri, and B. Maham, "Capacity and error probability analysis of neuro-spike communication exploiting temporal modulation," *IEEE Trans. Commun.*, vol. 68, no. 4, pp. 2078–2089, Apr. 2020.

[21] K. Aghababaiyan, V. Shah-Mansouri, and B. Maham, "Axonal channel capacity in neuro-spike communication," *IEEE Trans. Nanobiosci.*, vol. 17, no. 1, pp. 78–87, Jan. 2018.

[22] E. Balevi and O. B. Akan, "A physical channel model for nanoscale neuro-spike communications," *IEEE Trans. Commun.*, vol. 61, no. 3, pp. 1178–1187, Mar. 2013.

[23] A. L. Hodgkin and A. F. Huxley, "A quantitative description of membrane current and its application to conduction and excitation in nerve," *J. Physiol.*, vol. 117, no. 4, pp. 500–544, Aug. 1952.

[24] F. N. Quandt and F. A. Davis, "Action potential refractory period in axonal demyelination: A computer simulation," *Biol. Cybern.*, vol. 67, no. 6, pp. 545–552, Oct. 1992.

[25] C. Koch, *Biophysics of Computation: Information Processing in Single XNeurons*. Oxford, U.K.: Oxford Univ. Press, 2004.

[26] G. L. Adonias, A. Yastrebova, M. T. Barros, Y. Koucheryavy, F. Cleary, and S. Balasubramaniam, "Utilizing neurons for digital logic circuits: A molecular communications analysis," *IEEE Trans. Nanobiosci.*, vol. 19, no. 2, pp. 224–236, Apr. 2020.

[27] G. L. Adonias, H. Siljak, M. T. Barros, and S. Balasubramaniam, "Neuron signal propagation analysis of cytokine-storm induced demyelination," 2021, *arXiv:2103.03790*.

[28] N. T. Carnevale and M. L. Hines, *The NEURON Book*, 1st ed. New York, NY, USA: Cambridge Univ. Press, 2009.

[29] M. Hines, "NEURON and Python," *Frontiers Neuroinform.*, vol. 3, p. 1, Jan. 2009.

[30] Y. Dombrowski *et al.*, "Regulatory T cells promote myelin regeneration in the central nervous system," *Nature Neurosci.*, vol. 20, no. 5, pp. 674–680, May 2017.

[31] U. S. Bhalla, *Multi-Compartmental Models Neurons*. Dordrecht, The Netherlands: Springer, 2012, pp. 193–225.

[32] C. C. H. Cohen *et al.*, "Saltatory conduction along myelinated axons involves a periaxonal nanocircuit," *Cell*, vol. 180, no. 2, pp. 311–322, Jan. 2020.

[33] M. Veletić, P. A. Floor, Z. Babić, and I. Balasingham, "Peer-to-peer communication in neuronal nano-network," *IEEE Trans. Commun.*, vol. 64, no. 3, pp. 1153–1166, Mar. 2016.

[34] C. E. Shannon, "A mathematical theory of communication," *Bell Syst. Tech. J.*, vol. 27, no. 3, pp. 379–423, Jul./Oct. 1948.

[35] I. F. Akyildiz and J. M. Jornet, "The Internet of Nano-Things," *IEEE Wireless Commun.*, vol. 17, no. 6, pp. 58–63, Dec. 2010.

[36] M. Veletić, P. A. Floor, Y. Chahibi, and I. Balasingham, "On the upper bound of the information capacity in neuronal synapses," *IEEE Trans. Commun.*, vol. 64, no. 12, pp. 5025–5036, Dec. 2016.

[37] D. Malak, M. Kocaoglu, and O. B. Akan, "Communication theoretic analysis of the synaptic channel for cortical neurons," *Nano Commun. Netw.*, vol. 4, no. 3, pp. 131–141, 2013.

[38] B. B. Averbeck, "Poisson or not Poisson: Differences in spike train statistics between parietal cortical areas," *Neuron*, vol. 62, no. 3, pp. 310–311, May 2009.

[39] I. Chakravarti, R. Laha, and J. Roy, *Handbook of Methods of Applied Statistics: Techniques of Computation, Descriptive Methods, and Statistical Inference* (Wiley Series in Probability and Mathematical Statistics), vol. 1. Hoboken, NJ, USA: Wiley, 1967, pp. 392–394.

[40] J. Platkiewicz and R. Brette, "A threshold equation for action potential initiation," *PLoS Comput. Biol.*, vol. 6, no. 7, Jul. 2010, Art. no. e1000850.

[41] M. W. Levine and J. M. Shefner, "A model for the variability of interspike intervals during sustained firing of a retinal neuron," *Biophys. J.*, vol. 19, no. 3, pp. 241–252, Sep. 1977.

[42] M. S. Hamada, M. A. Popovic, and M. H. P. Kole, "Loss of saltation and presynaptic action potential failure in demyelinated axons," *Frontiers Cellular Neurosci.*, vol. 11, p. 45, Feb. 2017.